Effects of partial thermalization and secondary emission on the electron distribution function in Hall thrusters

IEPC-2005-118

Presented at the 29th International Electric Propulsion Conference, Princeton University, October 31 - November 4, 2005

E. Ahedo* and V. de Pablo†

Universidad Politécnica de Madrid, Madrid 28040, Spain

M. Martínez-Sánchez‡

Massachusetts Institute of Technology, Cambridge, MA 02139, USA

A one-dimensional, kinetic model of the electron population between the lateral walls of a Hall thruster is developed, with the aim assessing the effect of electron thermalization on the replenishment of the high-energy tails of the electron distribution function that are collected by the walls. Secondary electron emission beams are included too. A presheath/sheath formulation, with simplified presheath dynamics, is adopted and the charge saturation limit of the sheaths is taken into consideration. Asymptotic results for the high- and low-thermalization limits are presented and compared with existing models. The solution of the problem remains unclear for high secondary emission and intermediate thermalization.

I. Introduction

The performance and lifetime of a Hall thruster with dielectric walls is very affected by the plasma-wall interaction. This leads to plasma recombination, electron energy losses, wall collisionality, and ion sputtering.[1,2] Plasma recombination depends on the two-dimensional response of the bulk of the plasma ,[3] but electron energy losses and wall collisionality depend mainly on the sheaths created close to the walls;[4] finally, ion sputtering depends on the response of both presheath (i.e. bulk of the plasma) and sheaths. The main or primary electron population is confined between the two chamber walls by the electrostatic potential, except for the high-energy tail of the distribution function that is collected by the walls. In addition, there can be large secondary electron emission(SEE) from the walls.

Hobbs and Wesson[5] showed that the sheath potential fall decreases and the energy losses into the wall increase as the SEE yield increases. For a SEE yield close to 1, they showed that the sheath enters into a space-charge saturated regime, that prevents the vanishing of the electron-repelling sheaths and bounds the electron energy losses to the walls. The application of this model to Hall thrusters was proposed by Jolivet and Roussel.[6] Then, Ahedo,[4] starting from the Hobbs-Wesson model, derived a presheath/sheath model capable of quantifying the above four plasma-wall interaction phenomena. The application of this wall interaction expressions into simulations of the Hall thruster discharge[7,8] has shown excessive particle and energy losses and, consequently, unreasonably strong deterioration of performances.

*Associate Professor, Escuela Técnica Superior de Ingenieros Aeronáuticos, eduardo.ahedo@upm.es.

†Ph.D. Candidate, Escuela Técnica Superior de Ingenieros Aeronáuticos, valentin.depablo@gmail.com.

‡Professor, Department of Aeronautics & Astronautics, mmart@mit.edu.

The model of Ahedo[4] considered a complete replenishment of the high-energy electrons collected by the walls. However, recent works suggest (i) a significant depopulation of these high-energy electrons caused by an insufficiently fast thermalization,[9–11] and (ii) the partial re-collection by the walls of secondary electrons that do not interact with the rest of the plasma.[12] Both phenomena, which modify certainly the sheath potential fall and the energy losses, depend basically on the thermalization of the electron population. At present, the understanding and modelling of this phenomenon is poor because of the several electron population and collisional processes, the complex dynamics of the magnetized electrons, and the possible influence of plasma instabilities.

The purpose of this paper is to derive a simple kinetic model for electrons, capable of (a) evaluating the effect of partial electron thermalization on both the primary and secondary populations and (b) determining the resulting sheath potential fall and plasma-wall interaction magnitudes. Also, we aim to recover the low and total thermalization asymptotic limits, which will provide useful analytical expressions and will allow a comparison with our previous macroscopic models. Electron thermalization will be modelled simply by an 'average' frequency, independent of the electron velocity and position. The influence of the weak electric field of the presheath on the electron population is ignored here. This simplification weakens the consistency of the model somehow but, on the other hand, leads to a more tractable and comprehensive model while it keeps fully the effects of the two processes, thermalization and SEE, we intend to discuss here.

Section II presents the electron model, Sec. III obtains its formal solution, Sec. IV presents the boundary conditions required to close the model, and Sec. V presents asymptotic and numerical solutions. Conclusions are presented in Sec. VI.

II. The kinetic electron model

A. Formulation

A one-dimensional, stationary plasma confined between two planar, ceramic walls is considered (Fig. 1). The zero Debye length limit is invoked, leading to a two-scale structure, consisting of a quasineutral presheath and collisionless space-charge sheaths adjacent to the walls. The sheaths are discontinuity surfaces in the presheath scale. Symmetry is assumed, so that only half-channel is studied. Let point M be the channel median and points Q and W represent the sheath/presheath transition and the wall.

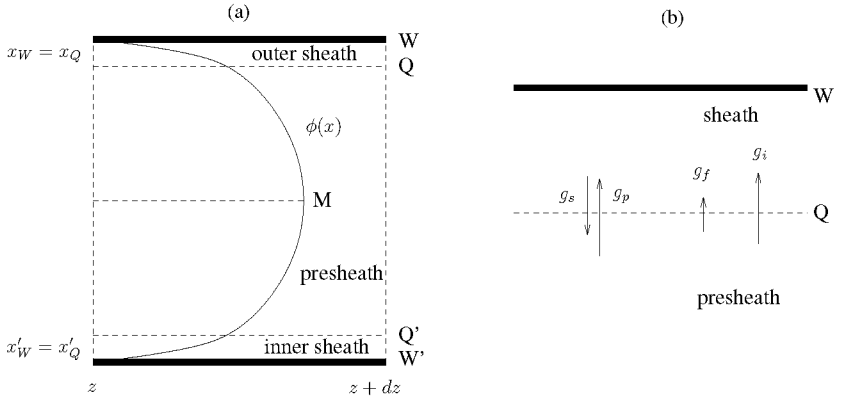

Figure 1. Sketch of the model.

The electric potential $\phi(x)$ is assumed monotonic in the half channel MW with $\phi_M = 0$ and $\phi < 0$ elsewhere. The only exception to this will be the very inner region of the sheath in the charge-saturation regime. We can take advantage of $\phi(x)$ being monotonic in region MW to use ϕ instead of x as independent variable and thus avoid the two spatial scales. The magnetic field is assumed perpendicular to the walls and all magnetic effects are disregarded.

The velocity of each electron is divided into components parallel and perpendicular to $\mathbf{1}_x$, $\boldsymbol{v} = v_x\mathbf{1}_x + v_\perp\mathbf{1}_\perp$ and the electron distribution function has the functional form $f(x, v_x, v_\perp)$. [Subscript e for electrons is

omitted in most variables.] This satisfies the Boltzmann equation

$$v_x \frac{\partial f}{\partial x} + \frac{e}{m_e}\frac{d\phi_x}{dx}\frac{\partial f}{\partial v_x} = \nu_e(f_0 - f) + \nu_i f_1 + \nu_z f, \tag{1}$$

where the terms on the right-hand side represent electron thermalization, ionization, and transverse diffusion. For convenience, when expressing the different contributions to this equation,

$$\varphi_p(v^2; T) = \left(\frac{m_e}{2\pi T}\right)^{p/2} \exp\left(-\frac{m_e v^2}{2T}\right) \tag{2}$$

represents a Maxwellian distribution function of temperature T in p dimensions.

Electron thermalization can be due to Coulomb collisions among electrons or fluctuation effects. A BGK formulation of this phenomenon uses a thermalization frequency ν_e and the local-equilibrium distribution function

$$f_0(\boldsymbol{x}, v) = n_e \varphi_3\Big((v_x - V_x)^2 + v_\perp^2; T_e\Big); \tag{3}$$

where n_e, V_x, and T_e are local density, fluid velocity, and temperature, respectively, defined in the usual way.

Gas ionization is modelled with a frequency ν_i and a Maxwellian distribution function for plasma production

$$f_1(\boldsymbol{x}, v) = n_e(x)\varphi_3(v^2, T_1), \tag{4}$$

and it can be assumed that $T_1 \ll T_0$. Finally, transverse (i.e. axial) diffusion of the plasma, is modelled with frequency ν_z and takes into account variations of the flow of the plasma parallel to the walls required to sustain the stationary radial discharge.

In addition, the model takes into consideration secondary electron emission(SEE) by electron impact at the walls. The SEE yield is modelled with a linear function

$$\delta(E) = \delta_0 + (1 - \delta_0)\frac{E}{E_1} \tag{5}$$

where $E = m_e v^2/2$ is the electron energy and E_1 is the electron energy for 100% SEE. The distribution function of secondary electrons at the wall (point W) is assumed semi-Maxwellian

$$f_{sW}(\boldsymbol{v}) = g_s \sqrt{\frac{2\pi m_e}{T_w}} \varphi_3(v^2, T_w) H(-v_x). \tag{6}$$

Here,

$$g_s \equiv -\int_{v_x<0} d\boldsymbol{v} v_x f_{sW} \tag{7}$$

is the secondary electron flux from the wall (with $g_s > 0$ for convenience) and $H(v)$ is the Heaviside step function. The determination of g_s in terms of the primary electron flux and the SEE yield is part of the solution.

The radial energy of each electron is conserved across the sheath:

$$m_e v_x^2/2 - e\phi = \text{const}. \tag{8}$$

Then, the distribution function of secondary electrons at the presheath boundary is $f_{sQ}(\boldsymbol{v}) = f_2(\boldsymbol{v})H(-v_x - v_{sh})$, with

$$f_2(\boldsymbol{v}) = g_s \sqrt{\frac{2\pi m_e}{T_w}} \exp\frac{e\phi_{WQ}}{T_w} \varphi_3(v^2, T_w), \tag{9}$$

and

$$v_{sh} = \sqrt{2e\phi_{WQ}/m_e} \tag{10}$$

the velocity increment across the sheath.

B. Simplifications

The analysis we present here is based on a simplified electron model. The main simplification is that we disregard the variations of the electric potential in the presheath (which amounts to take $\phi_Q = \phi_M$). Thus we will not be able to obtain a correct solution of the presheath. However, this simplification will not prevent us from studying the coupled roles of electron thermalization and SEE on the electron-wall interaction.

The two other simplifications are mainly a consequence of the previous one. First, we will neglect gas ionization, since cold electrons created from ionization cannot be treated properly without considering the potential variations in the presheath. And second, we substitute the local equilibrium function $f_0(v)$, Eq. (3), by the global one

$$f_0(\boldsymbol{v}) = n_0 \varphi_3(v^2; T_0), \tag{11}$$

where n_0 and T_0 are constant.

Taking integral moments over $\boldsymbol{v}$ on the Boltzmann equation, the radial electron flow g_e satisfies

$$\frac{dg_e}{dx} = \nu_e(n_o - n_e) + \nu_z n_e, \tag{12}$$

and the electron flux reaching the sheath and the wall is

$$g_{eQ} = g_{eW} = \nu_e \left(n_0 \frac{h}{2} - \int_0^{h/2} dx n_e \right) + \nu_z \int_0^{h/2} dx n_e. \tag{13}$$

Notice that in order that $f_0(v_0)$ does not contribute (globally) to the plasma production it must be

$$\frac{2}{h} \int_0^{h/2} n_e dx = n_0 \tag{14}$$

$$\nu_z = 2 g_{eW} / n_0 h. \tag{15}$$

This is the plasma balance equation[13] for this model, which, in the absence of ionization, determines the transverse contribution of plasma, i.e. ν_z. For any other value of ν_z, only Eq. (13) would be satisfied, n_0 would not be the mean value of n_e in the presheath, and there would be net plasma production associated to f_0.

III. Solution for the electron population

Let ϕ_{WQ} the sheath potential drop, which will be determined later as part of the solution.

A. Electron distribution function in presheath

Calling

$$\nu = \nu_e - \nu_z, \tag{16}$$

the general solution of Eq. (1) in the presheath, with the simplifications commented above, is

$$f(x, \boldsymbol{v}) = A(\boldsymbol{v}) \exp \frac{-\nu x}{v_x} + \frac{\nu_e}{\nu} f_0(v) \tag{17}$$

where $A(\boldsymbol{v})$ is to be determined from the boundary conditions at the sheath/presheath transition Q ($x_Q = h/2$) and the channel centerline M ($x_M = 0$). First, the symmetry condition at $x = x_M$ yields $f(0, -\boldsymbol{v}) = f(0, \boldsymbol{v})$. Second, at $x = x_Q$ particles with $0 < v_x < v_{sh}$, are reflected within the sheath. This means $f(x_Q, v_x) = f(x_Q, -v_x)$ for $|v_x| < v_{sh}$. Third, at $x = x_Q$, particles with $v_x < -v_{sh}$ correspond only to the SEE, that is $f(x_Q, \boldsymbol{v}) = f_2(\boldsymbol{v})$ for $v_x < -v_{sh}$.

Applying the above boundary conditions, the electron distribution function in the presheath is

$$f(x, \boldsymbol{v}) = \begin{cases} \dfrac{\nu_e}{\nu} f_0, & |v_x| < v_{sh}, \\ \dfrac{\nu_e}{\nu} f_0 + \left(f_2 - \dfrac{\nu_e}{\nu} f_0 \right) \exp \left[-\nu \left(\dfrac{x}{v_x} + \dfrac{h/2}{|v_x|} \right) \right], & |v_x| > v_{sh}. \end{cases} \tag{18}$$

B. Electron distribution function in sheath

Particularizing the distribution function at the sheath transition Q, one has

$$f_Q(v_x) = \begin{cases} f_2(v_x), & v_x < -v_{sh}, \\ \dfrac{\nu_e}{\nu} f_0(v_x), & |v_x| < v_{sh}, \\ \dfrac{\nu_e}{\nu} f_0(v_x) \left[1 - \exp\Big(-\dfrac{\nu h}{v_x}\Big)\right] + f_2(v_x) \exp\Big(-\dfrac{\nu h}{v_x}\Big), & v_x > v_{sh}, \end{cases} \tag{19}$$

where the dependence on $v_\perp$ is omitted for sake of simplicity. The radial energy of each electron is conserved across the sheath, Eq. (8). Using ϕ as a convenient independent variable for the sheath and

$$v_{xQ}(\phi, v_x) = \text{sign}(v_x)\sqrt{v_x^2 + 2e(\phi_Q - \phi)/m_e}, \tag{20}$$

the distribution function inside the sheath satisfies

$$f(\phi, v_x) = f_Q(v_{xQ}(\phi, v_x)). \tag{21}$$

C. Particle and energy fluxes across the sheath

The net flux of electrons at the wall W has three contributions:

$$g_{eW} = \int d\boldsymbol{v} v_x f_W(\boldsymbol{v}) \simeq g_p + g_f - g_s, \tag{22}$$

where (moving integration from W to point Q), g_s defined in Eq. (7),

$$g_p \simeq \int_{v_x > v_{sh}} d\boldsymbol{v} \Big(1 - \exp\frac{-\nu h}{v_x}\Big) v_x \frac{\nu_e}{\nu} f_0, \tag{23}$$

$$g_f = \int_{v_x > v_{sh}} d\boldsymbol{v} v_x f_2 \exp\frac{-\nu h}{v_x}, \tag{24}$$

are the contributions of 'secondary' electrons, 'primary' electrons, and 'free secondary' electrons coming from the opposite wall (at $x = -h/2$), respectively.

In a similar way, the flux of electron energy to the wall W is

$$q_{eW} = \int d\boldsymbol{v} \frac{1}{2} m_e v^2 v_x f_W = q_p + q_f - q_s, \tag{25}$$

where (proceeding similarly to g_{eW})

$$q_p \simeq \int_{v_x > v_{sh}} d\boldsymbol{v} \left(T_0 - e\phi_{WQ} + \frac{1}{2} m_e v_x^2\right) \Big(1 - \exp\frac{-\nu h}{v_x}\Big) v_x \frac{\nu_e}{\nu} f_0, \tag{26}$$

$$q_f = \int_{v_x > v_{sh}} d\boldsymbol{v} \left(T_w - e\phi_{WQ} + \frac{1}{2} m_e v_x^2\right) v_x f_2 \exp\frac{-\nu h}{v_x}, \tag{27}$$

$$q_s = 2T_w g_s, \tag{28}$$

are the contributions from primary and free-secondary electrons. We expect $q_p \sim T_0 g_p \gg q_s$ and $q_f < q_s$, so that $q_{eW} \simeq q_p$.

The flux of electrons at points Q and W are the same, but the electron energy flux at point Q is higher than at point W,

$$q_{eQ} = q_{eW} + e\phi_{WQ} g_{eW}, \tag{29}$$

where the last term includes non-negligible contributions from secondary electrons.

We use now Eq. (5) for the SEE yield in order to express g_s in terms of g_p. One has

$$g_s = \int_{v_x > 0} d\boldsymbol{v} v_x f_W \delta\left(\frac{m_e v^2}{2}\right) = \int_{v_x > v_{sh}} v_x f_Q \delta\left(\frac{m_e v^2}{2} - e\phi_{WQ}\right). \tag{30}$$

Then, it turns out easily that

$$g_s = \delta_0(g_p + g_f) + (1 - \delta_0)\frac{q_p + q_f}{E_1}, \tag{31}$$

so that the effective SEE yield can be expressed as

$$\frac{g_s}{g_p} = \frac{\delta(\alpha_p T_0)}{1 - \alpha_f \delta_0} \tag{32}$$

with $\alpha_f = g_f/g_s$ and $\alpha_p = q_p + q_f/T_0 g_p$; we will see below that $\alpha_p \sim 1.8 - 2$.

IV. Closure of the model

Ion dynamics in the presheath cannot be solved with the simplified model discussed here. Nevertheless, the ion flux at the sheath edge can be determined from conditions dictated by the sheath problem. The Poisson equation for the sheath potential is

$$\frac{d\phi}{dx^2} = \frac{e}{\epsilon_0}\left[n_e(\phi) - n_i(\phi)\right] \tag{33}$$

where the plasma densities depend only on ϕ because the sheath is collisionless. The development of a space-charge, monotonic solution at point Q require that

$$\frac{d}{d\phi}\left[n_e(\phi) - n_i(\phi)\right]_Q \geq 0, \tag{34}$$

which is the Bohm condition. Accepting that the ion flux fulfills the marginal (or sonic) form of the Bohm condition, and assuming that ions are singly charged and enter the sheath as a quasi-cold beam, one has

$$\frac{e n_{eQ}^3}{m_i g_{iW}^2} = \left.\frac{dn_e}{d\phi}\right|_Q, \tag{35}$$

where: conservation of the ion flux across the sheath and plasma quasineutrality have been applied, and g_{iW}/n_{eQ} is the ion fluid velocity at the sheath edge. This condition relates the ion flux to magnitudes that depend only on the electron model and thus avoids to solve the ion dynamics in the presheath. Indeed, Eq. (35) is a boundary condition for this problem. One expects to have

$$g_{iW} \sim n_0\sqrt{T_0/m_i} \tag{36}$$

The solution for the electron distribution function f depends on four groups of parameters. First, we have h, n_0, and T_0, which are the input parameters used commonly to non dimensionalize plasma equations and variables. Second, there is ν_e, which measures thermalization effects. Third, we have δ_0, E_1 and T_w, which model the SEE. And four, there are ϕ_{WQ} and ν_z which, in fact, are output parameters. This means that a doubly iterative process must be used to solve the problem. The two extra conditions that determine ϕ_{WQ} and ν_z are the following. First, the zero electric current condition at the wall means

$$g_W \equiv g_{iW} = g_{eW}. \tag{37}$$

Substituting here the electron and ion fluxes from Eqs. (22) and (35) we end with an implicit equation for ϕ_{WQ}. We will show that this implicit character can lead to a non-unique solution of the problem. Second, ν_z must verify (15).

One important restriction to the present model remains to be noted. All the study here has been based on a monotonic potential fall in the sheath. However, for high SEE the sheath can become charge-saturated. The charge-saturated limit(CSL) of the sheath correspond to attaining zero electric field at the wall boundary. In terms of electric charge within the sheath, the CSL is defined by

$$\int_{\phi_W}^{\phi_Q} (n_i - n_e) d\phi = 0 \tag{38}$$

The practical determination of the CSL is not simple since it implies one extra level of iteration and the computation of double integrals on the potential.

For cold SEE (i.e. $T_w \ll T_0$) the charge-saturated regime of the sheath is simple to visualize from the CSL. For warm SEE, the effects of the potential well formed near the wall need to be considered.

V. Results

Four thermalization regimes can be distinguished in our model:
a) high thermalization: $\nu_e h \gg v_{sh} = \sqrt{2e\phi_{WQ}/m_e}$;
b) intermediate thermalization, $\nu_e h = O(v_{sh})$;
c) low thermalization, $\sqrt{T_0/m_i} \ll \nu_e h \ll v_{sh}$; and
d) very low thermalization, $\nu_e h \leq O(\sqrt{T_0/m_i})$.
High thermalization is the case assumed by most models and simulations of Hall thrusters, but intermediate or low thermalization are more plausible for typical Hall thruster parameters (at least within this model hypotheses). For instance, for T_e = 20eV, $n_e = 10^{18}\text{s}^{-1}$ and h =15mm, one has $h^{-1}\sqrt{T_0/m_e} \simeq 1.2 \times 10^8\text{s}^{-1}$, $h^{-1}\sqrt{T_0/m_i} \sim 2.5 \times 10^5\text{s}^{-1}$, and the electron-electron thermalization frequency is[14] $\sim 2 \times 10^7\text{s}^{-1}$. which places ν_e in the low thermalization case. Turbulent effects could increase ν_e to the intermadiate thermalization case.

Next, we present first analytical solutions for the three asymptotic limits, and then numerical results for any thermalization level. These use T_0 instead of $e\phi_{WQ}$ to non-dimensionalize the thermalization frequency, $\hat{\nu}_e = \nu_e h\sqrt{m_e/T_0}$, which modifies slightly the ranges of the above thermalization cases.

A. High thermalization limit: $\nu_e h \gg v_{sh}$

It allows one to take $\exp(-\nu h/v_x) \simeq 0$ in Eq. (19).

From Eqs. (23), (24), and (26), we have

$$g_p = n_0\sqrt{\frac{T_0}{2\pi m_e}}\exp\left(-\frac{e\phi_{WQ}}{T_0}\right), \qquad g_f \simeq 0, \qquad q_p = 2T_0 g_p. \tag{39}$$

Then, the flux ratio between the different populations are

$$\frac{g_s}{g_p} = \delta(2T_0), \qquad \frac{g_p}{g_W} = \frac{1}{1-\delta(2T_0)}, \tag{40}$$

and from the expression of g_p the sheath potential fall satisfies

$$\frac{e\phi_{WQ}}{T_0} = \frac{1}{2}\ln\frac{m_i}{2\pi m_e} + \ln[1-\delta(2T_0)] + \frac{1}{2}\ln\frac{n_0^2 T_0}{m_i g_W^2}, \tag{41}$$

where the argument of the last logarithm can be expressed in terms of the plasma density, using the Bohm condition (35).

These results are valid as long as the CSL is not reached, that is for $1-\delta(2T_0) \gg \sqrt{m_e/m_i}$, roughly.

B. Low thermalization limits: $\nu_e h \ll v_{sh}$

In this case we take $\exp(-\nu h/v_x) \simeq 1-\nu h/v_x$. From Eqs. (23), (24), and (26), and calling $\hat{\phi}_{WQ} = e\phi_{WQ}/T_0$, one has

$$g_p \simeq \nu_e h\int_{v_{sh}}^{\infty} dv_x \tilde{f}_0 = \frac{1}{2}\nu_e h n_0 \text{erfc}(\hat{\phi}_{WQ}^{1/2}), \tag{42}$$

$$g_f = g_s - \nu h n_{sQ} = \left(1-\frac{\nu h}{v_{sh}}\right)g_s \simeq g_s, \tag{43}$$

$$q_p \simeq \nu_e h\int_{v_{sh}}^{\infty} dv_x \tilde{f}_0\left(T_0 - e\phi_{WQ} + \frac{m_e v_x^2}{2}\right) = (T_0 - e\phi_{WQ})g_p + h n_0 T_o\frac{\nu_e}{\sqrt{\pi}}\int_{\hat{\phi}_{WQ}^{1/2}}^{\infty} t^2 \text{e}^{-t^2} dt. \tag{44}$$

Then, the flux ratios are

$$\frac{g_s}{g_p} = \frac{\delta(\alpha_p T_0)}{1-\delta_0}, \qquad \frac{g_p}{g_W} = 1, \tag{45}$$

and the sheath potential fall satisfies

$$\mathrm{erfc}\sqrt{\frac{e\phi_{WQ}}{T_0}} = \frac{2g_W}{\nu_e h n_0}, \tag{46}$$

where again Eq. (35) must be used for g_W.

From Eq. (44), the energy flux of primary electrons satisfies

$$\frac{q_p}{T_0 g_p} = \frac{3}{2} + \left[\frac{\hat{\phi}_{WQ}^{1/2}\exp(-\hat{\phi}_{WQ})}{\sqrt{\pi}\mathrm{erfc}(\hat{\phi}_{WQ}^{1/2})} - \hat{\phi}_{WQ}\right] = 2 - \frac{1}{2\hat{\phi}_{WQ}} + O(\hat{\phi}_{WQ}^{-2}) \tag{47}$$

The above expressions are valid for $\nu_e h \geq O(\sqrt{T_0/m_i})$. For $\nu_e h \gg \sqrt{T_0/m_i}$, one has $\hat{\phi}_{WQ} \gg 1$ and some extra asymptotic expressions can be used.

Notice that, except for high SEE, the case $\nu_e h \sim \sqrt{T_0/m_e}$ presents $e\phi_{WQ}/T_0 \sim \ln\sqrt{m_i/m_e} \gg 1$ and $\nu_e h \ll \sqrt{e\phi_{WQ}/m_e}$, so it still verifies the low thermalization asymptotic expressions.

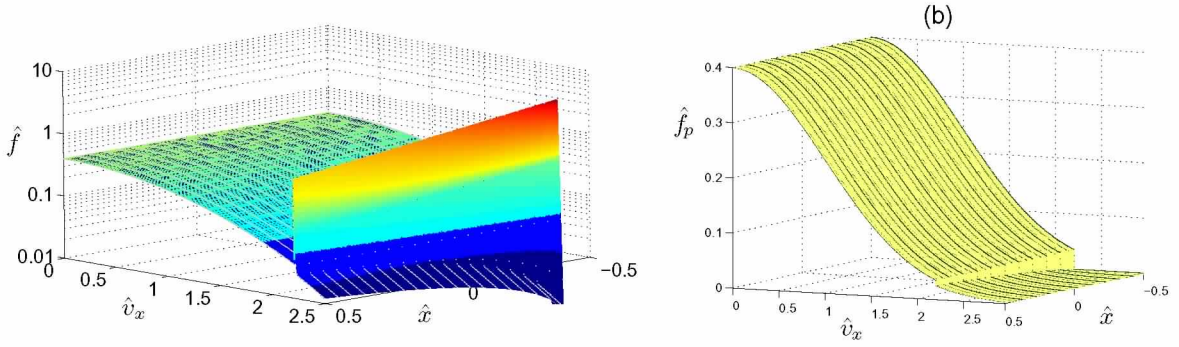

Figure 2. (a) Spatial evolution of the electron distribution function [$\hat{f}(\hat{x},\hat{v}_x) = n_0^{-1}\sqrt{T_0/m_e}\int f d\boldsymbol{v}_\perp$, $\hat{x} = x/h$, $\hat{v}_x = v_x\sqrt{m_e/T_0}$] for $\nu_e h\sqrt{m_e/T_0} = 2.8027$ and $T_0/E_1 = 0.667$. Output parameters: $e\phi_{WQ}/T_0 = 2.4251$, $g_s/g_p = 1.2882$, and $g_f/g_s = 0.2814$. In (b) the beam of secondary electrons has been omitted.

C. Numerical results

Figure 2 shows the evolution of the electron distribution function, along the channel for a case of intermediate thermalization; the evolution within the sheaths is not shown. For $v_x < 0$, take $f(x,v_x) = f(-x,-v_x)$. The secondary electron beam coming from the wall lying next to $x = -0.5$, reaches the presheath with the velocity v_{sh} and is then partially thermalized. At $x/h = -0.5$, there are no primary electrons with $v \geq v_{sh}$; this tail is partially replenished within the presheath and then collected at the wall next to $x/h = 0.5$.

Figure 3(a)-(f) show the combined effects of (i) thermalization and (ii) SEE on the plasma parameters. For low and high thermalization frequencies the numerical results recover the asymptotic limits analyzed above. For high thermalization (i.e. for $\hat{\nu}_e \gg 1$ in Fig. 3) : secondary electrons are thermalized while crossing the channel leading to $g_f \to 0$; both g_p/g_W and ϕ_{WQ} depend strongly on the SEE yield and not on ν_e; the flux of electron energy satisfies $q_{eW} \simeq 2T_0 g_p$; and the Bohm condition for the ion flux yields $g_W \simeq n_0\sqrt{T_Q/m_i}$. For low thermalization (i.e. for $\hat{\nu}_e = \nu_e h/\sqrt{T_0/m_e} \ll 1$ in Fig. 3) : secondary electrons cross almost freely the channel; the flux ratio between primary electrons and ions remains close to 1, independently of the SEE; and ϕ_{WQ} grows with ν_e and is independent of the SEE. This low-thermalization behavior was predicted by Ahedo and Parra.[12]

For low thermalization, $q_{eW}/2T_0 g_p$ decreases mildly from 1, as predicted by Eq. (47). Fig. 3(f) shows that the temperature of the electron distribution function at the sheath entrance, T_{eQ}, is lower than T_0 because of the depletion of high-energy primary electrons. Of course, this effect is more pronounced for low thermalization and near the CSL. Fig. 4 compares the temperatures at points M and Q; the differences are negligible for low thermalization since f remains almost invariant along the presheath. Notice that Fig. 3(b) plots the plasma flux to the wall g_W normalized with the electron temperature at point Q. The Bohm condition (35) leads to $g_W \simeq n_0\sqrt{T_{eQ}/m_i}$. The discrepancies from this law are larger for low thermalization

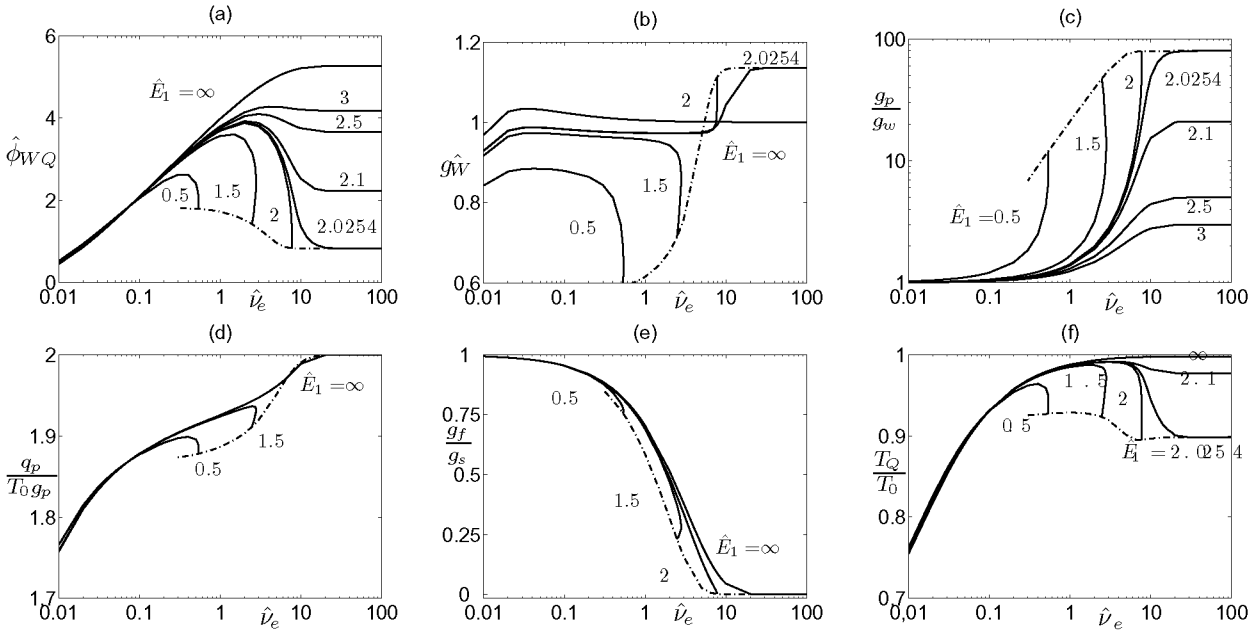

Figure 3. Evolution of plasma parameters with the thermalization frequency ($\hat{\nu}_e = \nu_e h\sqrt{m_e/T_0}$) for different values of the SEE yield: $\hat{E}_1 = E_1/T_0 = \infty$, 3, 2.5, 2.1, 2.0254, 2, 1.5, and 0.5. Other input parameters: $\delta_0 = 0$, $T_w/T_0 = 0.01$, and $\sqrt{m_e/m_i} = 489.18$. The dash-dot line represents the charge-saturation limit. (a) Sheath potential fall, $\hat{\phi}_{WQ} = e\phi_{WQ}/T_0$, (b) ion flux, $\hat{g}_W = g_W/(n_0\sqrt{T_Q/m_i})$, (c) particle flux ratio between primary electrons and ions, (d) relative energy flux of primary electrons, (e) particle flux ratio between free-secondary to total-secondary electrons, and (f) electron temperature at point Q.

and the CSL. The transverse plasma diffusion or contribution is measured by ν_z. From Eq. (15), this frequency is proportional to the plasma deposition at the wall, g_W. One has

$$\nu_z = \frac{2g_W}{n_0 h} \sim 2\frac{\sqrt{T_0/m_i}}{h} \tag{48}$$

so that $\nu_z \ll \nu_e$ except for very low thermalization. This means that transverse diffusion plays almost no role on the determination of $f(x, \boldsymbol{v})$; it just serves to fulfill the global particle conservation.

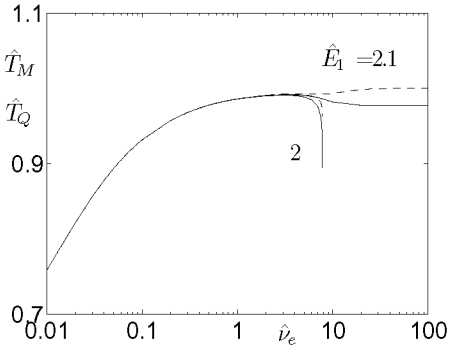

Figure 4. Comparison of electron temperatures at points M (dashed lines) and Q (solid lines), $\hat{T} = T/T_0$, for different thermalization and SEE cases.

Based on Fig. 3(a), Fig. 5 allows one to obtain the non-simple evolution of the sheath potential fall with the plasma temperature, before the CSL is reached. For high thermalization there is a monotonic decrease of ϕ_{WQ} with T_0, whereas the trend is just the opposite for low thermalization. For intermediate thermalization

the situation is more complex. First, $\phi_{WQ}(T_0)$ presents a relative maximum. Second, there is a thin range of values of T_0/E_1, where two solutions of the problem exist, both without sheath charge-saturation (this is clearly seen in Fig. 3 too). Then, for larger values of T_0/E_1 there is no solution (except perhaps a charge-saturated one). Mathematically, the double-solution and the no-solution cases are consequences of the influence of ϕ_{WQ} on the ion flux g_{iW}, through the Bohm condition (35). This makes implicit the equation that determines ϕ_{WQ}, as Eqs. (41) and (46) for the two asymptotic limits illustrate. At present, we still ignore whether this double-solution is physically plausible and the way the plasma selects one solution or another. The lack of a non-CSL solution for high thermalization and high SEE must be further investigated too.

In the limit $\hat{\nu}_e \to \infty$ (and xenon), the CSL is reached for $E_1/T_0 \simeq 2.0254$, that is $g_s/g_p \simeq 0.9875$. Hobbs and Wesson[5] found $g_s/g_p \simeq 0.983$, the differences with our model consisting on they used (i) a full Maxwellian function for the primary electrons at the sheath edge and (ii) the limit $T_w = 0$; Ahedo and Parra used these Hobbs-Wesson hypotheses too. The difference can look small in terms of g_s/g_p but it amounts to a 24% in terms of both g_p/g_W and electron energy losses. As the thermalization frequency decreases, Fig. 6 shows that the CSL is reached for lower values of E_1/T_0 and larger values of the SEE yield, a trend already found by Ahedo and Parra.[12] Notice that Fig. 6(b) here compares well with their Fig. 4.

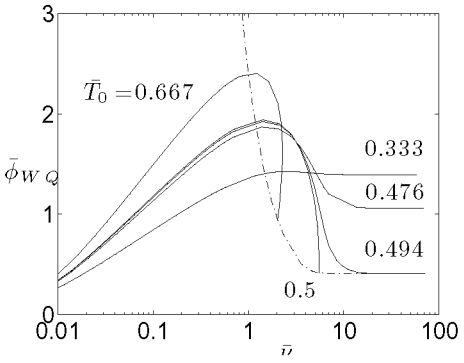

Figure 5. Evolution of the sheath potential fall ($\bar{\phi}_{WQ} = e\phi_{WQ}/E_1$) vs the thermalization frequency ($\bar{\nu}_e = \nu_e h\sqrt{m_e/E_1}$) for different electron temperatures, $\bar{T}_0 = T_0/E_1$. Notice that E_1 is used to nondimensionalize all magnitudes. The dash-dot line represents the charge-saturation limit.

Finally, Fig. 6(a)-(c) shows that the emission temperature of secondary electrons T_w has some effect on the plasma response. In particular, the sheath potential fall at the CSL decreases and the region of non-CSL in Fig. 6(a) decreases slightly.

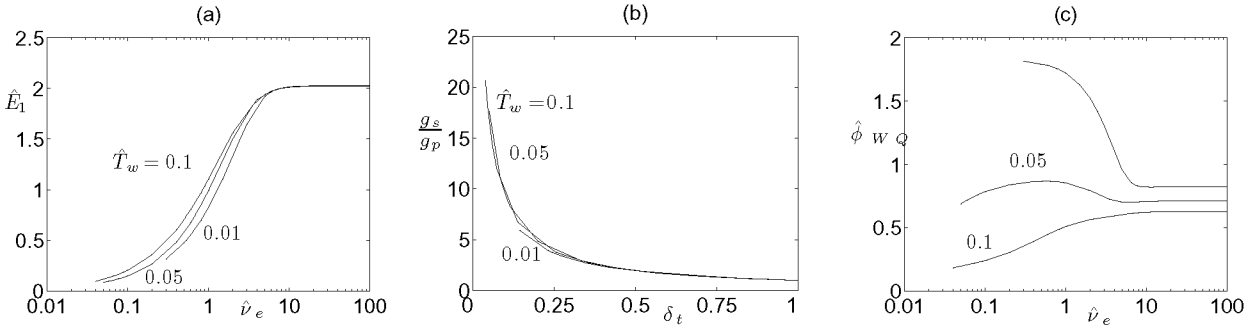

Figure 6. Parameters of the charge saturation limit(CSL) and the influence of the emission temperature of secondary electrons, $\hat{T}_w = T_w/T_0$. (a) SEE yield vs thermalization frequency; (b) SEE yield vs relative fraction of trapped-secondary electrons, $\delta_t = 1 - g_f/g_s$; (c) sheath potential fall.

VI. Conclusions

The kinetic formulation presented here is able to model the depletion and partial replenishment of the high-energy tails of primary electrons collected by the walls, which was a feature missed by the models of Hobbs and Wesson and of Ahedo for high thermalization, and of Ahedo and Parra for low thermalization.

The main accomplishments have been to determine: (i) the evolution of the primary-tail replenishment and the SEE trapping with the thermalization frequency, (ii) the anode sheath fall and the fluxes of particles and energy to the walls, (iii) the influence of thermalization on the charge-saturation limit, and (iv) the asymptotic solutions for high and low thermalization (confirming for this last case the SEE-trapping model of Ahedo-Parra).

The most novel and unexpected result we have found is the response for intermediate thermalization and high SEE, where parametric intervals with two (non-CSL) solutions exist. This parametric region needs more further research to understand whether it is just a consequence of the model assumptions or it is plausible physically.

The present model has neglected the effect produced by the presheath potential fall on the electron distribution function. The consideration of this aspect is very important to improve the reliability and accuracy of the model, and to analyze the matching between the presheath and sheath solutions. This matching should lead to confirm or not the Bohm condition, which has a central role on the existence of double solutions commented above. The extension of the model to obtain the distribution function for charge-saturated sheaths can also be necessary to understand the mystery of the double solutions.

The main phenomenon (Coulomb collisions or fluctuations) governing the electron thermalization is, of course, a key aspect of the problem we pretend to the understand, and requires its own research, which should provide the functional dependence of the thermalization frequency to be used in the electron kinetic model.

Finally, it must be noticed that other collisional processes, like the electron-neutral elastic collisions, do not thermalize the electron distribution function but affect it. In particular, they modify the SEE beams and the collectable primary-tails, and thus the sheath characteristics.

Acknowledgments

This work was sponsored by the Ministerio de Educación y Ciencia of Spain (Project ESP2004-03093).

References

[1]V. Zhurin, H. Kaufman, and R. Robinson, Plasma Sources Sci. Technol. **8**, R1 (1999).

[2]A. Morozov and V. Savelyev, *Reviews of Plasma Physics*, volume 21, chapter 2, Kluwer Academic, New York, 2000.

[3]E. Ahedo, Physics of Plasmas **9**, 3178 (2002).

[4]E. Ahedo, Physics of Plasmas **9**, 4340 (2002).

[5]G. Hobbs and J. Wesson, Plasma Physics **9**, 85 (1967).

[6]L. Jolivet and J.-F. Roussel, Effects of the secondary electron emission on the sheath phenomenon in a Hall thruster, in *SP-465: 3rd Spacecraft Propulsion Conference, Cannes(Francia)*, pp. 367–376, Noordwijk, The Netherlands, 2000, European Space Agency.

[7]E. Ahedo, J. Gallardo, and M. Martínez-Sánchez, Physics of Plasmas **10**, 3397 (2003).

[8]F. Parra, E. Ahedo, M. Martínez-Sánchez, and M. Fife, A two-dimensional hybrid model of the Hall thruster discharge, (to be submitted).

[9]N. Meezan and M. Capelli, Physical Review E **66**, 036401 (2002).

[10]O. Batishev and M. Martínez-Sánchez, Charge particle transport in the Hall effect thruster, in *Proc. 28th International Electric Propulsion Conference, Toulouse, France*, Electric Rocket Propulsion Society, Cleveland, OH, 2003.

[11]K. Sullivan, J. Fox, O. Batischev, and M. Martínez-Sánchez, Kinetic study of wall effects in SPT, in *40th Joint Propulsion Conference, Fort Lauderdale, FL*, AIAA-2004-3777, American Institute of Aeronautics and Astronautics,Washington, DC, 2004.

[12]E. Ahedo and F. Parra, Physics of Plasmas **12**, 073503 (2005).

[13]L. Tonks and I. Langmuir, Physical Review **34**, 876 (1929).

[14]R. Goldston and P. Rutherford, *Introduction to Plasma Physics*, Institute of Physics Publishing, Bristol, 1995.